HEALTH AND MEDICINE

Articular fibrocartilage-targeted therapy by microtubule stabilization

Jiawei Li[1], Huiming Jiang[2], Zhongyang Lv[1], Ziying Sun[1], Chaoqun Cheng[3], Guihua Tan[1], Maochun Wang[1], Anlong Liu[1], Heng Sun[1], Hu Guo[1], Fufei Chen[1], Zizheng Liu[1], Yuxiang Fei[1], Yuan Liu[1], Rui Wu[1], Xingquan Xu[1], Wenjin Yan[1], Qing Jiang[1], Dongquan Shi[1]*

The fibrocartilage presented on the joint surface was caused by cartilage injury or degeneration. There is still a lack of effective strategies for fibrocartilage. Here, we hypothesized that the fibrocartilage could be viewed as a raw material for the renewal of hyaline cartilage and proposed a previously unidentified strategy of cartilage regeneration, namely, "fibrocartilage hyalinization." Cytoskeleton remodeling plays a vital role in modifying the cellular phenotype. We identified that microtubule stabilization by docetaxel repressed cartilage fibrosis and increased the hyaline cartilage extracellular matrix. We further designed a fibrocartilage-targeted negatively charged thermosensitive hydrogel for the sustained delivery of docetaxel, which promoted fibrocartilage hyalinization in the cartilage defect model. Moreover, the mechanism of fibrocartilage hyalinization by microtubule stabilization was verified as the inhibition of Sparc (secreted protein acidic and rich in cysteine). Together, our study suggested that articular fibrocartilage-targeted therapy in situ was a promising strategy for hyaline cartilage repair.

INTRODUCTION

Hyaline cartilage is the specific type of cartilage located at the joint surface (*1*). The extracellular matrix (ECM) of hyaline cartilage mainly consisted of collagen fibers [mainly type II collagen (Col II)], glycosaminoglycans (GAGs), and water (*2*), which enable hyaline cartilage compressive and frictional features. The therapy of cartilage injuries remains a challenge because of its poor regenerative ability and the inevitable development to posttraumatic osteoarthritis (OA) (*3*). During cartilage restoration, aberrant collagen expression could result in the formation of fibrocartilage (*1*, *4*). In many cases, a rudimentary repaired fibrocartilage showed the inferior mechanical properties (*3*, *5*). Physiological fibrocartilage is naturally present in vertebral discs, meniscus, pubic symphysis, and the tendon-bone interface (*6*). However, the fibrocartilage presented in the joint during OA or during cartilage injuries was a result of cartilage fibrosis (*7*). Then, fibrocartilage in the synovial joint, which lacks its original function, even worsens the symptoms of OA (*8*). However, there is still a lack of effective resolution on articular fibrocartilage in cartilage injury.

When disease occurs, hyaline cartilage chondrocytes become actively proliferative in the lesion to respond to the stimuli in the microenvironment (*1*, *9*). The proliferative chondrocytes undergo a drastic change in cellular function, metabolism, and cytoskeleton, eventually contributing to the increased expression of Col I (*10*). While loading, the electrostatic and steric interactions of hyaline cartilage prevent water loss and bear most of the load. The dense and fibril ECM of fibrocartilage does not exhibit this structure-function relationship (*11*). However, as a self-repaired product of cartilage injury, we believed that fibrocartilage has the following advantages: (i) Its ECM could be viewed as an autologous scaffold for cartilage repair, (ii) containing the natural cell source for hyaline cartilage renewal, and (iii) integrating well with surrounding cartilage or subchondral bone. Therefore, we hypothesized that the fibrocartilage could be viewed as a raw material for the renewal of hyaline cartilage. The strategies must be addressed that focus on reducing the fibrotic markers and improving the hyaline cartilage phenotype of the fibrotic chondrocytes (FCs) and ECM in fibrocartilage.

Here, we proposed a previously unidentified strategy in cartilage repair focusing on the modification of existing fibrocartilage into hyaline cartilage, namely, "fibrocartilage hyalinization." The key of this strategy is modifying the local cells (FCs) and utilization of the original ECM in the defect to improve their hyalinization (Fig. 1A). Cytoskeleton remodeling affects protein synthesis and secretion, which, in turn, sets the direction of differentiation (*12*). As one important member of the cytoskeleton, microtubule plays a vital role in regulating the proteins assembling and the intracellular transportation (*13*, *14*). Microtubule always undergoes the constant remodeling through alternating growth and shrinkage (*15*). However, the "catastrophe" events of microtubule occurred when cells suffer rapid stimulation or mechanical stress alteration. The stability of microtubules can provide the long life and the extension of microtubules to ensure their basic functions (*14*). Much attention was attracted to microtubule as pathologic mechanism or therapeutic target for the disease, such as spinal cord injury, Alzheimer's disease, and myocardial dysfunction (*16*–*19*). Several reports showed that the microtubule stabilizer, docetaxel or paclitaxel, prevented the progression of rheumatoid arthritis in rats or patients (*20*). Our recent work demonstrated that microtubule stabilization improved chondrogenesis and inhibited the expression of Col I in synovial mesenchymal stem cells (MSCs) (*21*). However, its role in

[1]State Key Laboratory of Pharmaceutical Biotechnology, Division of Sports Medicine and Adult Reconstructive Surgery, Department of Orthopedic Surgery, Affiliated Nanjing Drum Tower Hospital, Nanjing University Medical School Nanjing, Nanjing, 210008 Jiangsu, P.R. China. [2]Department of Sports Medicine and Adult Reconstructive Surgery, The Affiliated Nanjing Hospital of Nanjing Medical University, Nanjing, 210000 Jiangsu, P.R. China. [3]Department of Biomedical Engineering, College of Engineering and Applied Sciences, Nanjing National Laboratory of Microstructures, Jiangsu Key Laboratory of Artificial Functional Materials, Nanjing University, Nanjing, 210023 Jiangsu, P.R. China.
*Corresponding author. Email: shidongquan@nju.edu.cn

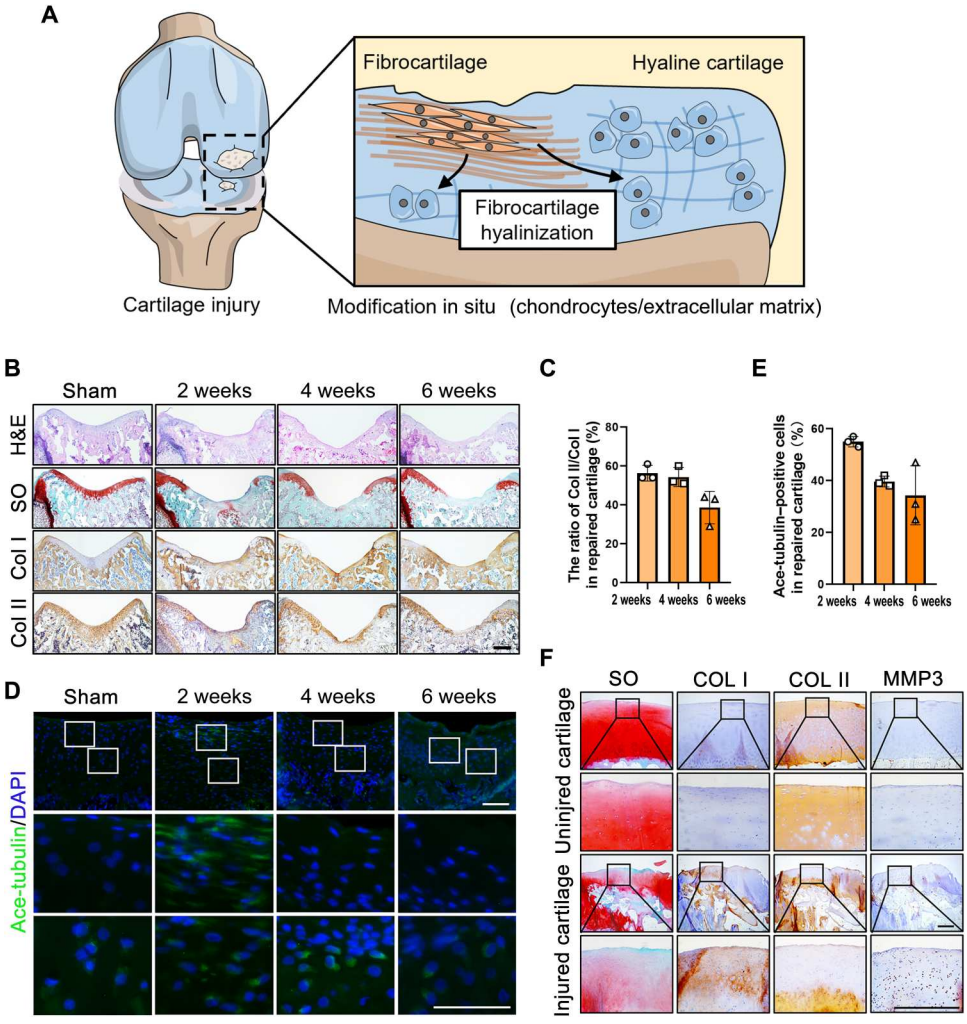

Fig. 1. Schematic of fibrocartilage hyalinization and the role of fibrocartilage in synovial joint. (**A**) Schematic illustration of fibrocartilage hyalinization. The key is the modification in situ of FCs and fibril ECM. (**B**) Representative hematoxylin and eosin staining (H&E), Safranin O (SO)–Fast Green, and immunohistochemical staining for Col I and Col II of the fibrocartilage in cartilage defect (2, 4, and 6 weeks after surgery) and the control (sham operation) groups. Scale bar, 500 μm. (**C**) Quantification of the ratio of the positive area of Col II to Col I based on (B) ($n = 3$). (**D**) Immunofluorescent staining for ace-tubulin of the fibrocartilage in cartilage defect (2, 4, and 6 weeks after surgery) and the control (sham operation) group. Scale bar, 200 μm. Enclosed areas are enlarged in below panels. (**E**) Quantification of the ace-tubulin–positive cells based on (D) ($n = 3$). (**F**) SO staining and immunohistochemical staining for COL I, COL II, and MMP3 of the human OA cartilage (uninjured and injured cartilage). Scale bar, 500 μm. Enclosed areas are enlarged in below panels. Data are presented as the means ± SD.

cartilage injury or fibrocartilage is still largely unclear. In the present study, we verified that microtubule stabilization was effective for inhibiting fibrosis and promoting hyalinization of fibrocartilage. Together, this study highlighted the feasibility of fibrocartilage modification in situ and presented microtubule stabilization as a promising approach for fibrocartilage hyalinization.

RESULTS

Fibrocartilage is formed after cartilage injury

To investigate the natural procedure of fibrocartilage regeneration, a full-thickness cartilage defect was constructed in the femoral trochlear of rats. During the cartilage restoration, we observed that the cells regenerated in the defect exhibited clustered distribution (Fig. 1B and fig. S1A). Furthermore, Col I was continuously expressed from early stage (2 weeks after injury) to relatively late stage (6 weeks after injury). Meanwhile, although Col II was observed during cartilage repair, the ratio of Col II to Col I was significantly decreased in the late stage (Fig. 1, B and C). It has been well recognized that FCs are the major source of these fibril proteins in the ECM of fibrocartilage (*6*). The arrangement of the cytoskeleton regulated the chondrocyte differentiation (*12*). The microtubule stability, represented by the expression of ace-tubulin, of the cells in cartilage defect was also down-regulated in fibrocartilage formation (Fig. 1, D, and E). Moreover, in the human OA cartilage samples harvested from knee joint, a high level of matrix metalloproteinase-3 (MMP3) was observed in the area with inferior COL II/I expression, indicating the detrimental effect of fibrocartilage on other cartilage tissues (Fig. 1F). These data suggest that the formation of fibrocartilage in cartilage repair is inevitable, and its existence further threatens the surrounding healthy tissue.

The identification of CTGF- and TGF-β1–induced FC

The acquirement of stable FCs was the first challenge before the investigation of fibrocartilage hyalinization in vitro. Previous studies reported that the stem cells induced by connective tissue growth factor (CTGF) and transforming growth factor–β (TGF-β) were effective for fibrocartilage regeneration (*22*, *23*). We speculated that CTGF and TGF-β treatment would be a practical approach for producing FCs. After preparing the bone marrow MSCs (BMSCs), we treated the cells with CTGF and TGF-β1 for 1 week sequentially to acquire induced FCs (iFCs) (Fig. 2A).

To identify the fibrotic phenotype of iFCs, we performed RNA sequencing of controlled BMSCs (BMSC_Ctrl) and CTGF- and TGF-β1–induced BMSCs (BMSC_C+T). A total of 5397 genes were differentially expressed with 2695 up-regulated and 2702 down-regulated among them (BMSC_C+T versus BMSC_Ctrl) (fig. S1B). As shown in the Venn graph, 10,842 genes were overlapped in two groups (fig. S1C). The heatmap showed the differentially expressed genes (Fig. 2B). The fibrosis-related genes were increased in iFCs, including *Col1a1*, *Col1a2*, *Col3a1*, *Fmod*, and *Fndc1*. The previously reported cartilage protective genes were decreased, including *Frzb*, *Fgfr3*, and *Fgf2* (*24*–*26*). Moreover, the gene set enrichment analysis (GSEA) illustrated that the Gene Ontology (GO) items of cell differentiation, extracellular space, growth factor activity, and developmental process were highly enriched in BMSC_Ctrl (Fig. 2C). However, the BMSC_C+T was more engaged in tumor necrosis factor receptor binding, cell redox homeostasis, exopeptidase activity, and regulation of catalytic activity (Fig. 2C).

After being induced by CTGF and TGF-β1, the cartilage development–associated proteins including Sox9 and Col II were down-regulated and the fibrotic proteins including Col I, Col III, and α–smooth muscle actin (α-SMA) were significantly up-regulated (Fig. 2D and fig. S2A). Co-immunofluorescence staining of F-actin and α-SMA also revealed the up-regulation of the α-SMA density after CTGF and TGF-β1 treatment (Fig. 2E). The ace-tubulin was also disturbed after CTGF and TGF-β1 treatment (Fig. 2, D and F, and fig. S2A). By flow cytometry analysis, we found that only CD44 was decreased after fibrosis inducing (Fig. 2G and fig. S2B). These results indicate that iFCs were successfully induced by the sequentially CTGF and TGF-β1 treatment and exhibit decreased microtubule stability.

Microtubule stabilization inhibits fibrosis and improves chondrogenesis of iFCs

After stable iFCs being acquired by sequential CTGF and TGF-β1 treatment, we investigated the role of microtubule remodeling in hyalinization. We used a microtubule stabilization reagent, docetaxel, to treat iFCs (Fig. 3A). The cell viability was inhibited when the concentration of docetaxel was higher than 5 nM (fig. S1B). Therefore, we chose 2.5 nM docetaxel to treat iFCs in the following research. The transcriptomic analysis illustrated that a total of 853 differentially expressed genes were found with 452 up-regulated and 401 down-regulated between docetaxel versus vehicle groups (fig. S1E). A total of 11,945 genes were overlapped in these two groups (fig. S1F). The fibrosis-related genes including *Fmod*, *Col1a1*, *Col3a1*, and *Fndc1* were markedly decreased, and the cytoskeleton-related genes including *Acta2*, *Tuba1a*, *Tuba4a*, and *Tubb2b* were substantially increased by the docetaxel treatment (Fig. 3B). GSEA showed that the items including extracellular region, receptor ligand activity, signaling receptor binding, and defense response were more enriched with docetaxel treatment (Fig. 3C).

The ace-tubulin was remarkably propelled with the docetaxel treatment in iFCs (Fig. 3, D and E, and fig. S2C). In contrast to vehicle group, docetaxel significantly improved the protein level of Sox9 and Col II (Fig. 3D and fig. S2C). Meanwhile, the fibrotic proteins were restrained by microtubule stabilization (Fig. 3E and fig. S2C). Consistently, the ratio of the α-SMA was lower in the docetaxel-treated group compared with the vehicle group (Fig. 3F). To clarify the role of microtubule stabilization on ECM formation in iFCs, we performed the micro-mass and pellet culture of iFCs. The results of safranin O (SO) staining and Alcian blue staining showed that more GAGs were synthesized in the cells treated by docetaxel (Fig. 3G). Moreover, the dense toluidine blue and SO staining in microtubule-stabilized pellet indicated that it was more inclined to produce the hyaline cartilage–like ECM (Fig. 3H). These data suggest that improving microtubule stabilization by docetaxel plays an effective role in transforming the iFCs to hyaline chondrocytes.

The synthesis and characterization of fibrocartilage-targeted docetaxel-loaded hydrogel scaffold

Abundant chondroitin sulfate mucopolysaccharide chains located in matrix endow the cartilage surface with a strong negative electrostatic effect (*27*). Our result suggested that a remarkable high expression of transferrin was observed in the fibrocartilage formed during cartilage repair (Fig. 4C). Transferrin was reported as a positively charged protein due to its carrier of iron ions (*28*). The transferrin in fibrocartilage provided a molecular target for drug carriers with negative surface charge.

Here, we designed a novel material that the docetaxel-loaded poly(lactic-*co*-glycolic acid)–1,2-distearoyl-*sn*-glycero-3-phosphoethanolamine–polyethylene glycol (PLGA-DSPE-PEG) nanoparticles (NPs) were encapsulated inside the methylcellulose hydrogel (D-PDP@MC-Gel) for the sustained release of docetaxel toward fibrocartilage after its intra-articular injection (Fig. 4, A and B). Docetaxel was encapsulated in the biodegradable PLGA NPs via an emulsion-based formulation approach. The DSPE-PEG was not only used to enhance the colloidal stability but also introduced a negative potential for the PLGA NPs.

The thermosensitive MC-Gel was then used to form an in situ formed hydrogel scaffold under physiological temperature. Scanning electron microscopy (SEM) displayed the spherical shapes of control PLGA-DSPE-PEG particles without docetaxel (PDP-particles) and particles with docetaxel (D-PDP-particles), as well as porous structure of MC-Gel (fig. S3A). As shown in Fig. 4E, when the storage modulus (G') was larger than loss modulus (G''), the gels were then formed into an elastic status. Both PDP@MC-Gel and D-PDP@MC-Gel showed a sol-to-gel transition at approximately 29°C. The strain and frequency examination indicated that the mechanical property of D-PDP@MC-Gel was slightly stronger than PDP@MC-Gel (fig. S3B). In addition, the gels reversed to solution form again when the temperature decreased, and repeated temperature rising and falling had no influence on its temperature response performance (Fig. 4F). Furthermore, the zeta potential of two types of particles was about −38 mV (Fig. 4G).

We then examined the adhesion of negatively charged MC-Gel to fibrocartilage in a rat cartilage injury model at 4 weeks after

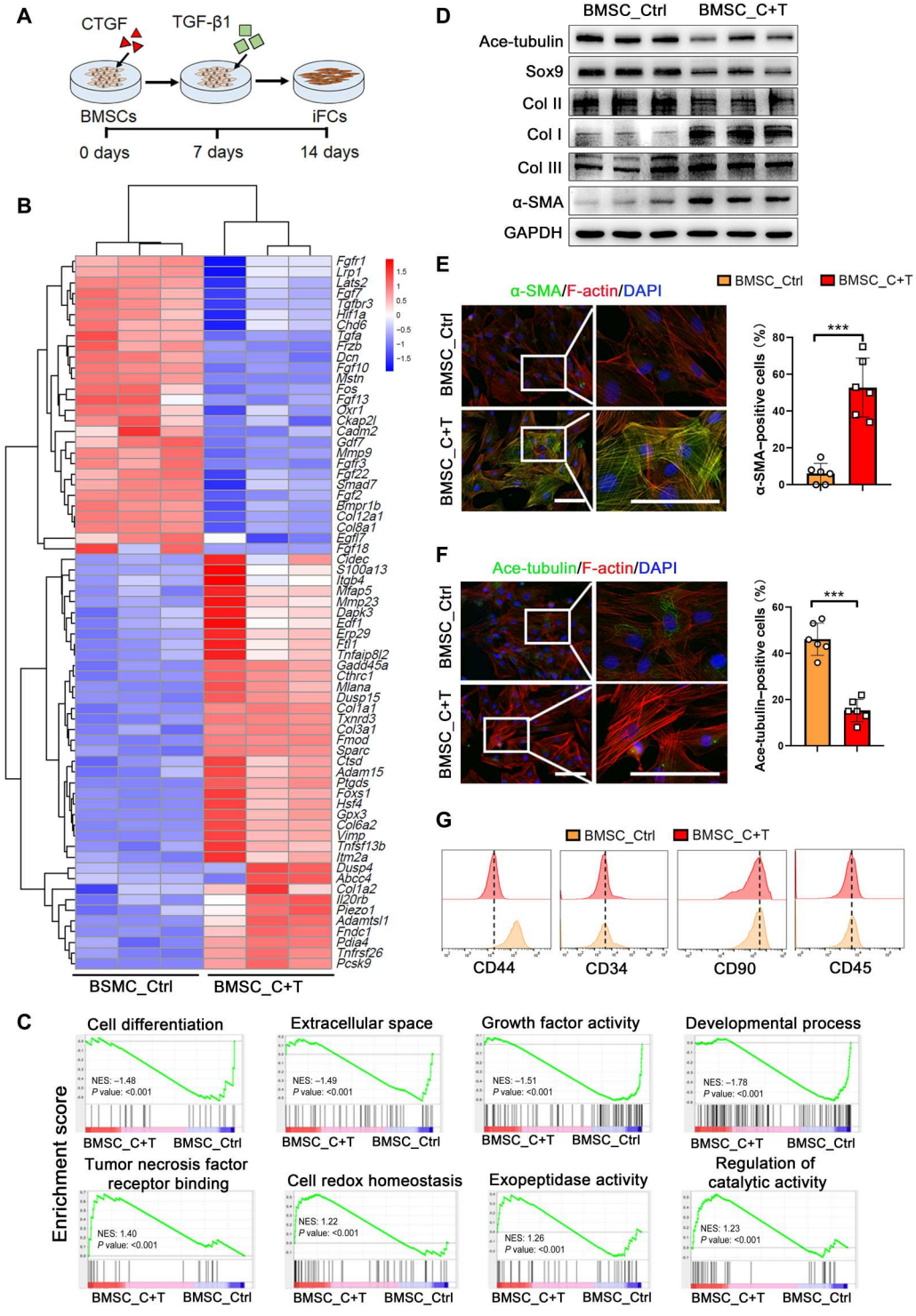

Fig. 2. The identification of CTGF- and TGF-β1–induced fibrocartilage chondrocytes. (**A**) Schematic illustration of the induction of FCs via CTGF and TGF-β1. The rat BMSCs were applied with CTGF (100 ng/ml) and TGF-β1 (10 ng/ml) for 1 week, respectively, to induce FCs. (**B**) Heatmap representing differential expression genes of cells (BMSC_C+T versus BMSC_Ctrl). Fibrosis-related genes were increased, including *Col1a1*, *Col1a2*, *Col3a1*, *Fmod*, and *Fndc1*, and cartilage protective genes were decreased, including *Frzb*, *Fgfr3*, and *Fgf2*. (**C**) GSEA showing the enrichment of pathways between the BMSC treatment with or without CTGF and TGF-β1 treatment. NES, normalized enrichment score. (**D**) Western blot analysis of ace-tubulin, Sox9, Col II, Col I, Col III, and α–smooth muscle actin (α-SMA) in BMSC treated with or without CTGF and TGF-β1 treatment. GAPDH, glyceraldehyde-3-phosphate dehydrogenase. (**E**) Co-immunofluorescent staining of α-SMA and F-actin in BMSC treated with or without CTGF and TGF-β1 treatment. Enclosed areas are enlarged in right panels. Scale bar, 100 μm. Quantification of the α-SMA–positive cells ($n = 6$). (**F**) Co-immunofluorescent staining of ace-tubulin and F-actin in BMSC treated with or without CTGF and TGF-β1 treatment. Enclosed areas are enlarged in right panels. Scale bar, 100 μm. Quantification of the ace-tubulin–positive cells ($n = 6$). (**G**) Peak graphs representing the flow cytometric analysis for CD44, CD34, CD90, and CD45 in BMSC treated with or without CTGF and TGF-β1 treatment. Data are represented as the means ± SD. ***$P < 0.001$.

surgery. The femur trochlear was removed from rat at 1 and 7 days after intra-articular injection with fluorescein isothiocyanate (FITC)–PDP@MC-Gel and imaged using a PerkinElmer In vivo Imaging System. The sample isolated at 1 day showed great retention of fluorescence in the whole articular surface, while the fluorescence was retained at the cartilage defect with fibrocartilage at 7 days after injection (Fig. 4H). These data provided evidence that the thermosensitive D-PDP@MC-Gel preferentially adhered to the fibrocartilage by electrostatic interaction. In addition, docetaxel levels at different time intervals following immersing in saline at 37°C were examined through high-performance liquid chromatography (HPLC). D-PDP@MC-Gel had a significantly higher concentration of docetaxel than D-PDP (Fig. 4I). These data provide evidence that the thermosensitive D-PDP@MC-Gel preferentially

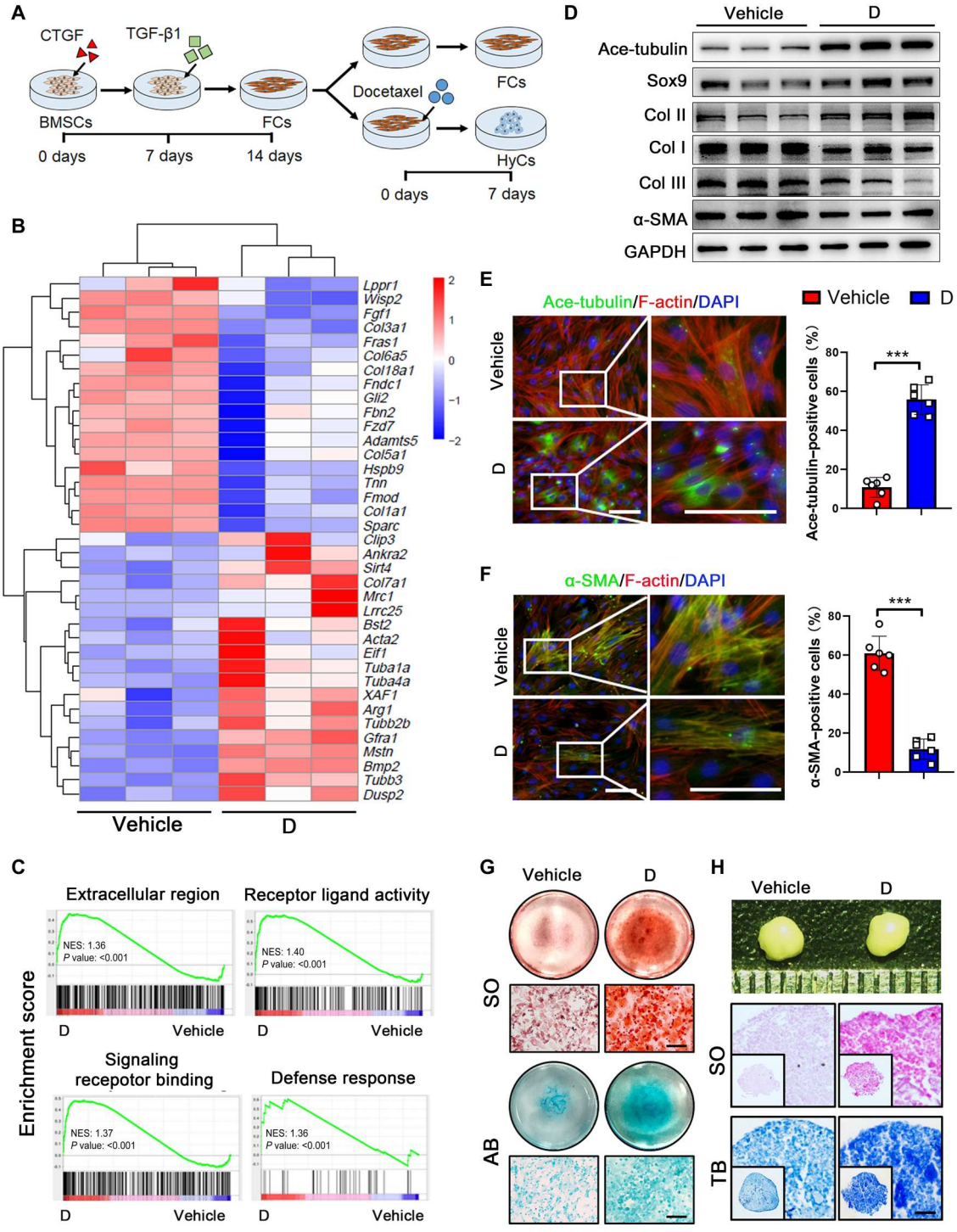

Fig. 3. Microtubule stabilization inhibits fibrosis and improves chondrogenesis of induced fibrocartilage chondrocytes. (**A**) Schematic illustration of the treatment for induced fibrocartilage chondrocytes (iFCs) with docetaxel (D) (2.5 nM) to stabilize microtubule of cells. (**B**) Heatmap representing differential expression genes of cells (D versus vehicle). The fibrosis related genes, including *Fmod*, *Col1a1*, *Col3a1*, and *Fndc1* were inhibited and the cytoskeleton related genes, including *Acta2*, *Tuba1a*, *Tuba4a*, and *Tubb2b* were increased by D treatment. (**C**) GSEA showing the enrichment of pathways between the iFCs with or not with D. (**D**) Western blot analysis of ace-tubulin, Sox9, Col II, Col I, Col III, and α-SMA in iFCs treated with or without D treatment. (**E**) Co-immunofluorescent staining of ace-tubulin and F-actin in iFCs treated with or without D treatment. Enclosed areas are enlarged in right panels. Scale bar, 100 μm. Quantification of the ace-tubulin–positive cells ($n = 6$). (**F**) Co-immunofluorescent staining of α-SMA and F-actin in iFCs treated with or without D treatment. Enclosed areas are enlarged in right panels. Scale bar, 100 μm. Quantification of the α-SMA–positive cells ($n = 6$). (**G**) SO staining and Alcian blue (AB) for the micro-mass culture of iFCs with or without D treatment. Scale bars, 200 μm. (**H**) Macroscopic image, SO staining, and toluidine blue (TB) staining for the pellet culture of iFCs with or not with D treatment. Scale bars, 200 μm. Microtubule stabilization improved the iFCs to produce the hyaline cartilage–like ECM. Data are represented as the means ± SD. ***$P < 0.001$.

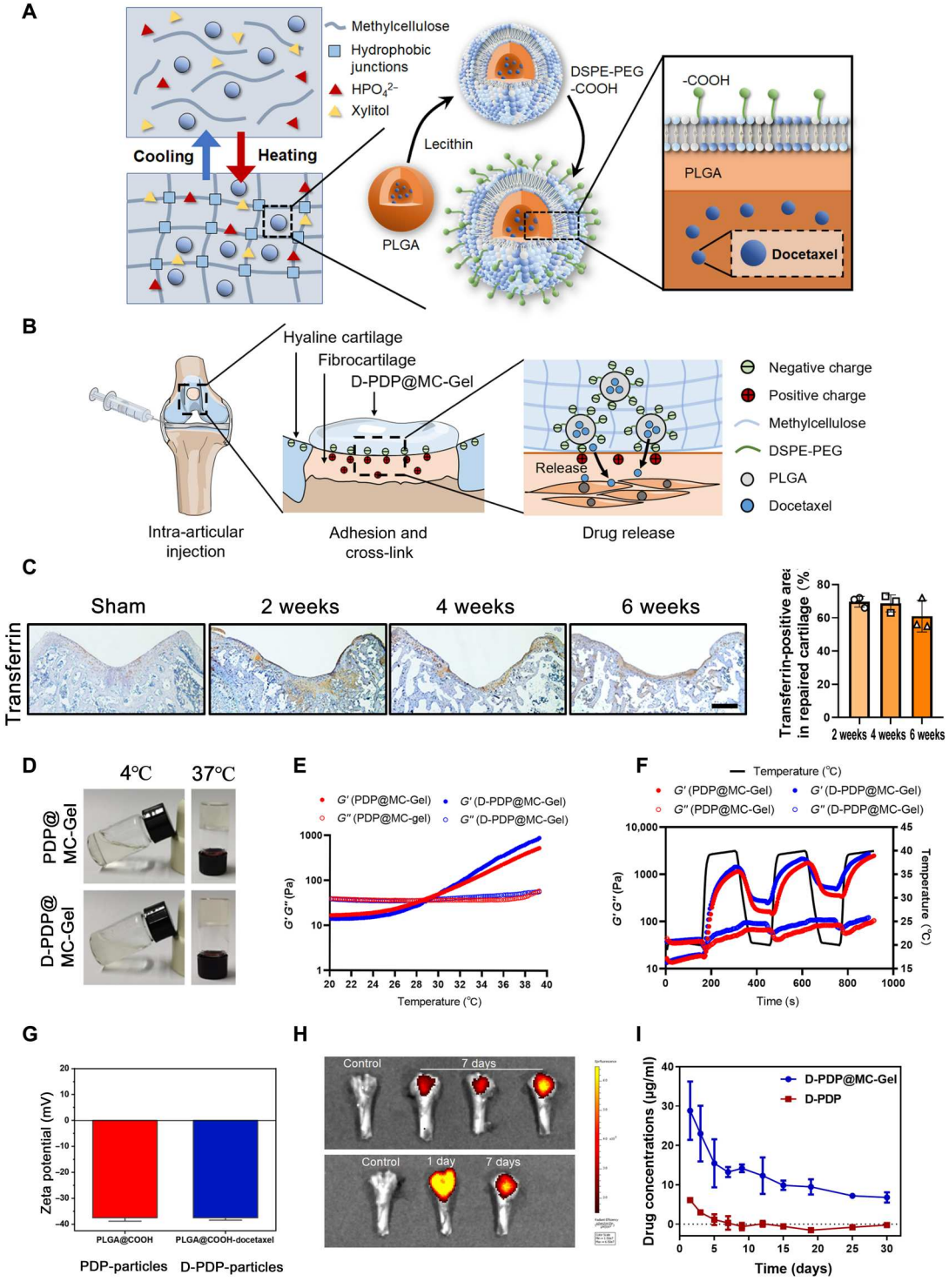

Fig. 4. Characterization of thermosensitive docetaxel loaded injectable hydrogel. Schematic illustration showing (**A**) the synthesis of thermosensitive docetaxel loaded injectable hydrogel (D-PDP@MC-Gel) and (**B**) the application of D-PDP@MC-Gel for fibrocartilage modification in situ. PLGA, poly(lactic-*co*-glycolic acid). (**C**) Immunohistochemical staining for transferrin of the fibrocartilage in cartilage defect (2, 4, and 6 weeks after surgery) and the control (sham operation) group. Scale bar, 200 μm. (**D**) Photographs of D-PDP@MC-Gel and the gel without docetaxel (PDP@MC-Gel) at 4 and 37°C. (**E** and **F**) Rheological test on D-PDP@MC-Gel and PDP@MC-Gel under different temperature. (**G**) Zeta potentials of D-PDP@MC-Gel and PDP@MC-Gel. (**H**) Images of fluorescence captured from the cartilage after the injection of FITC-PDP@MC-Gel 1 and 7 days. (**I**) In vitro drug concentrations of D-PDP@MC-Gel and D-PDP in saline at 37°C. The amount of D remaining in the solution released from the D-PDP and D-PDP@MC-Gel.

adheres to the fibrocartilage by electrostatic interaction and continuously releases docetaxel.

Docetaxel-loaded injectable hydrogel promotes fibrocartilage hyalinization in vivo

To verify the effect of D-PDP@MC-Gel on fibrocartilage hyalinization in vivo, we constructed a rat cartilage injury model and performed an intra-articular injection of the control gels and different dosage docetaxel-loaded gels (5, 10, and 25 μg/kg) when fibrocartilage formed (4 weeks after surgery) (Fig. 5A). First, we found that the low dosage of docetaxel, including 5 and 10 μg/kg, did not have a significant effect on changing the ECM of fibrocartilage (fig. S4A). However, docetaxel (25 μg/kg) in hydrogel increased the content of GAGs in fibrocartilage (fig. S4A). Therefore, we chose the fibrocartilage-targeted hydrogel loading docetaxel (25 μg/kg) for further research in vivo. Moreover, we performed the intra-articular injection of docetaxel without fibrocartilage-targeted hydrogel in to rat cartilage injury model. Significantly, there was no difference in the cell organization, and the morphological character of the tissue in knee joint, including meniscus and synovium, was not observed between each group (fig. S4B). The examination of key organs histology and the weight difference of rats revealed no obvious toxicity of docetaxel and MC-Gels to animals (figs. S3C and S4C). As shown in the macroscopic image, the D-PDP@MC-Gel–treated cartilage exhibited more smooth and intact filling in the surface than the control group and PDP@MC-Gel–treated group (Fig. 5B). More intact subchondral bone formation by D-PDP@MC-Gel treatment was observed by three-dimensional (3D) reconstruction of micro–computed tomography (micro-CT) images (Fig. 5B and fig. S4F). Obviously, the histological results indicated the organized cell distribution and abundant GAGs in the cartilage defect area of D-PDP@MC-Gel treatment group (Fig. 5, C and E). The chondrocytes in cartilage defect treated with D-PDP@MC-Gel showed higher expression of ace-tubulin (Fig. 5, D and F). Furthermore, by observing the border of defect, it was found that the ace-tubulin was specifically increased in fibrocartilage, illustrating the effect of docetaxel targeting to fibrocartilage by negatively charged gel (fig. S3, D and E). The ratio of Col II/I in the repaired tissue in defect area was significantly improved by D-PDP@MC-Gel treatment (Fig. 5, G to I). The matrix changed in fibrocartilage in the docetaxel-loaded gel-treated group also included decreased level of Fmod and increased level of aggrecan (Fig. 5, J to M). These results indicate the promising effect of D-PDP@MC-Gel in transforming fibrocartilage to hyaline cartilage in situ.

Microtubule stabilization improves the hyalinization of human fibrocartilage in OA

To determine the role of microtubule stabilization in fibrocartilage hyalinization in human OA cartilage, we harvested the degenerated cartilage from a patient with OA and treated it with or without docetaxel (Fig. 6A). After incubated with docetaxel for 1 week, the ace-tubulin in chondrocytes was remarkably increased than the control group (Fig. 6, B to E). Meanwhile, the level of SOX9 and COL II were significantly improved by docetaxel treatment (Fig. 6, D and E). The histological results revealed that docetaxel treatment significantly ameliorated the ratio of COL II/I (Fig. 6, F and G). In addition, FMOD was down-regulated and aggrecan was up-regulated in the microtubule stabilization group (Fig. 6, H and I). These data identify the effect of microtubule stabilization in transforming human fibrocartilage into hyaline cartilage in OA.

The inhibition of Sparc is involved in fibrocartilage hyalinization by microtubule stabilization

The expression of *Sparc* (secreted protein acidic and rich in cysteine) was increased in the fibrotic process and decreased with the docetaxel treatment in the results of RNA sequencing (Figs. 2B and 3B). The protein-protein interaction (PPI) analysis indicated that the Sparc is related to the fibrotic proteins in the CTGF- and TGF-β1–inducing and microtubule-stabilizing processes (Fig. 7A). Moreover, the cytoskeletal genes showed a relationship with fibrosis process in the docetaxel treatment of iFCs (Fig. 7A). It was indicated that Sparc might be involved in the fibrocartilage formation and abolished by microtubule stabilization. Sparc expression was increased by CTGF and TGF-β1 treatment and decreased by docetaxel treatment in vitro (Fig. 7, B to G). We knocked down the expression of Sparc by small interfering RNA (siRNA) in BMSCs when induced by CTGF and TGF-β1 and then found that the fibrosis was inhibited and that the chondrogenesis was increased (Fig. 7, H and I). The deficiency of Sparc showed the similar effect with docetaxel treatment on repressing the fibrotic phenotype of iFCs (fig. S5, A and B). The Sparc expression was increased during fibrocartilage formation in the cartilage defect (Fig. 7J). However, compared with the control and the PDP@MC-Gel groups, Sparc was inhibited by D-PDP@MC-Gel in the fibrocartilage in vivo (Fig. 7K). In the human cartilage, docetaxel also depressed Sparc expression as compared with the control group (Fig. 7L). Furthermore, we observed that the expression of CTGF was also enhanced during cartilage repair, while docetaxel treatment significantly inhibited its expression (fig. S5, C to F). These results suggest that Sparc and CTGF promote fibrocartilage production, and hence, the inhibition of Sparc and CTGF can be the therapeutic targets in fibrocartilage hyalinization.

DISCUSSION

A previously unidentified strategy named fibrocartilage hyalinization, which focused on fibrocartilage modification in situ, was proposed in this study. Here, we explored the method to establish the in vitro and in vivo model of fibrocartilage formation and demonstrated that microtubule stabilization of FCs improved the fibrocartilage hyalinization through inhibiting Sparc (Fig. 8). Moreover, a thermosensitive docetaxel-loaded hydrogel was constructed to target fibrocartilage and successfully achieved the fibrocartilage hyalinization in the rat cartilage injury model (Fig. 8).

The status of microtubule (stabilized and destabilized) determines the cell organization and several signaling pathways (*13*). In recent decades, the development of microtubule stabilization agents has made great contribution to clinical cancer research and treatment (*29*). Most of them were used in clinical applications, such as paclitaxel, docetaxel, epothilones, and taccalonolides (*29*). On the basis of its multifunction, microtubule stabilization has also attracted numerous attention in the clinical and basic research of other diseases (*13*, *14*). In this study, we treated iFCs with a classic microtubule-stabilizing agent, docetaxel. On the basis of this, we first aimed at fibrocartilage modification through regulating the microtubule stability of iFCs. Microtubule stabilization inhibited the fibrotic phenotype and induced the expression of hyaline

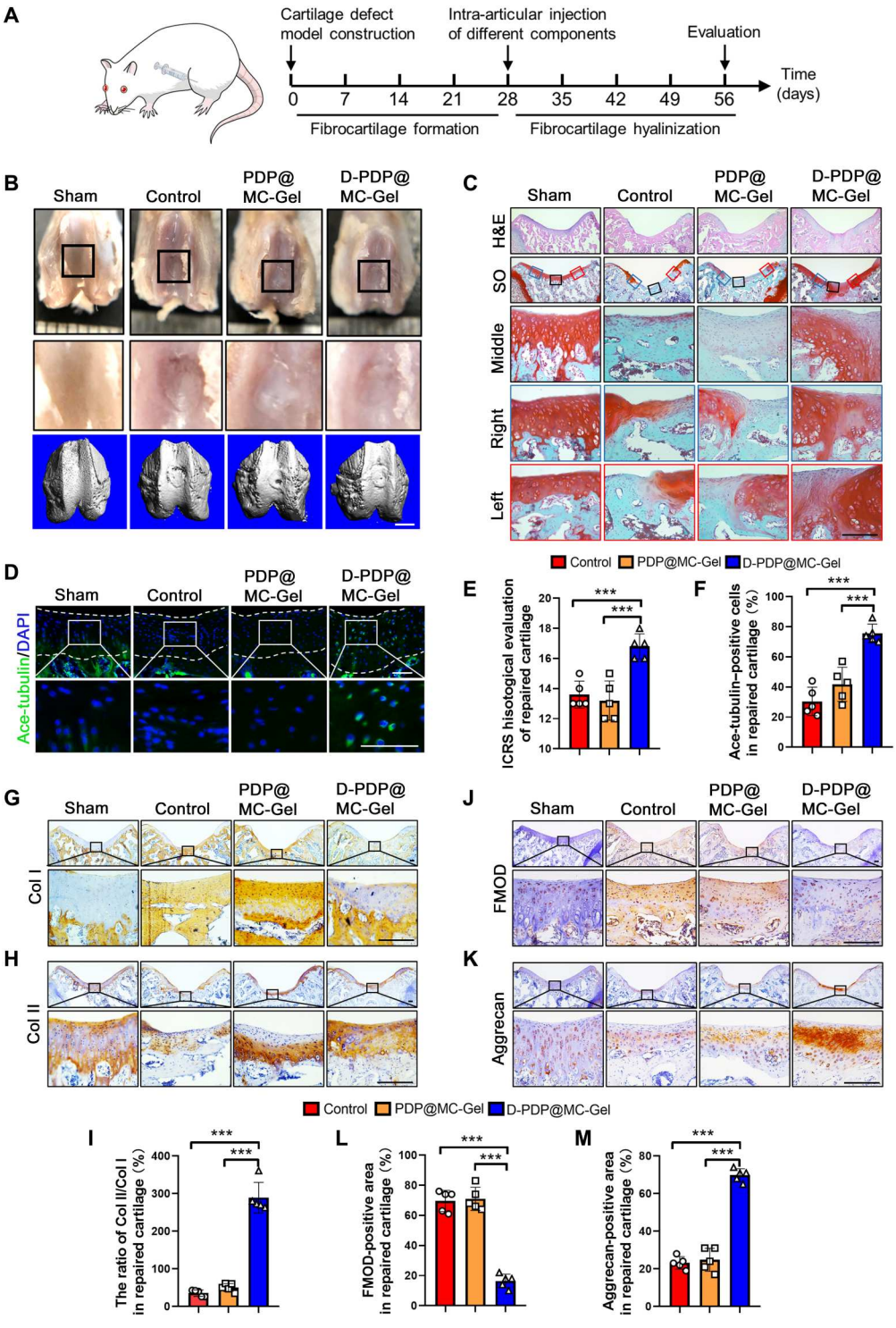

Fig. 5. The effect of thermosensitive docetaxel loaded injectable hydrogel in fibrocartilage in vivo. (**A**) Overview of animal experiments. (**B**) Macroscopic appearance and micro-CT 3D reconstruction of the fibrocartilage in the cartilage defect treated with D-PDP@MC-Gel and PDP@MC-Gel. White scale bar, 2 mm. Enclosed areas are enlarged in below panels. (**C**) H&E and SO staining of the fibrocartilage in the cartilage defect treated with D-PDP@MC-Gel and PDP@MC-Gel. Enclosed areas represent the middle, left and right of cartilage defect and are enlarged in below panels. Scale bar, 100 μm. (**D**) Immunofluorescent staining of ace-tubulin of the fibrocartilage in the cartilage defect treated with D-PDP@MC-Gel and PDP@MC-Gel. Enclosed areas are enlarged in below panels. Scale bar, 100 μm. (**E**) Histological ICRS evaluation of cartilage regeneration based on (C) ($n = 5$). ICRS, International Cartilage Repair Society. (**F**) Quantification of ace-tubulin–positive cells in the fibrocartilage in the cartilage defect ($n = 5$). (**G** to **K**) Immunohistochemical staining for Col I (G), Col II (H), FMOD (J), and aggrecan (K) of the fibrocartilage in the cartilage defect treated with D-PDP@MC-Gel and PDP@MC-Gel. Enclosed areas are enlarged in below panels. Scale bars, 100 μm. (**I** to **M**) Quantification of the ratio of Col II to Col I of (G) and (H), the Fmod-positive cells of (J), and the aggrecan-positive cells of (K) ($n = 5$). Data are represented as the means ± SD. ***$P < 0.001$.

cartilage–related protein in iFCs. It was suggested that FCs showed the potential of transforming into hyaline chondrocytes and microtubule stabilization was a promising target for FC modification in situ. Moreover, we identified the effect of microtubule stabilization on human OA cartilage. The human OA cartilage treated with docetaxel ex vivo also exhibited increased hyaline cartilage phenotype and inhibited fibrocartilage phenotype. These data verify that microtubule stabilization played an important role in inducing fibrocartilage hyalinization. However, most microtubule stabilization agents are toxic and have side effects, such as neurotoxicity, hematological toxicity, and diarrhea (*30*). Our results showed that the cell viability and proliferation were inhibited by high concentrations of docetaxel (>2.5 nM). Therefore, further investigations on optimal concentration, dosing intervals, and duration of therapy are

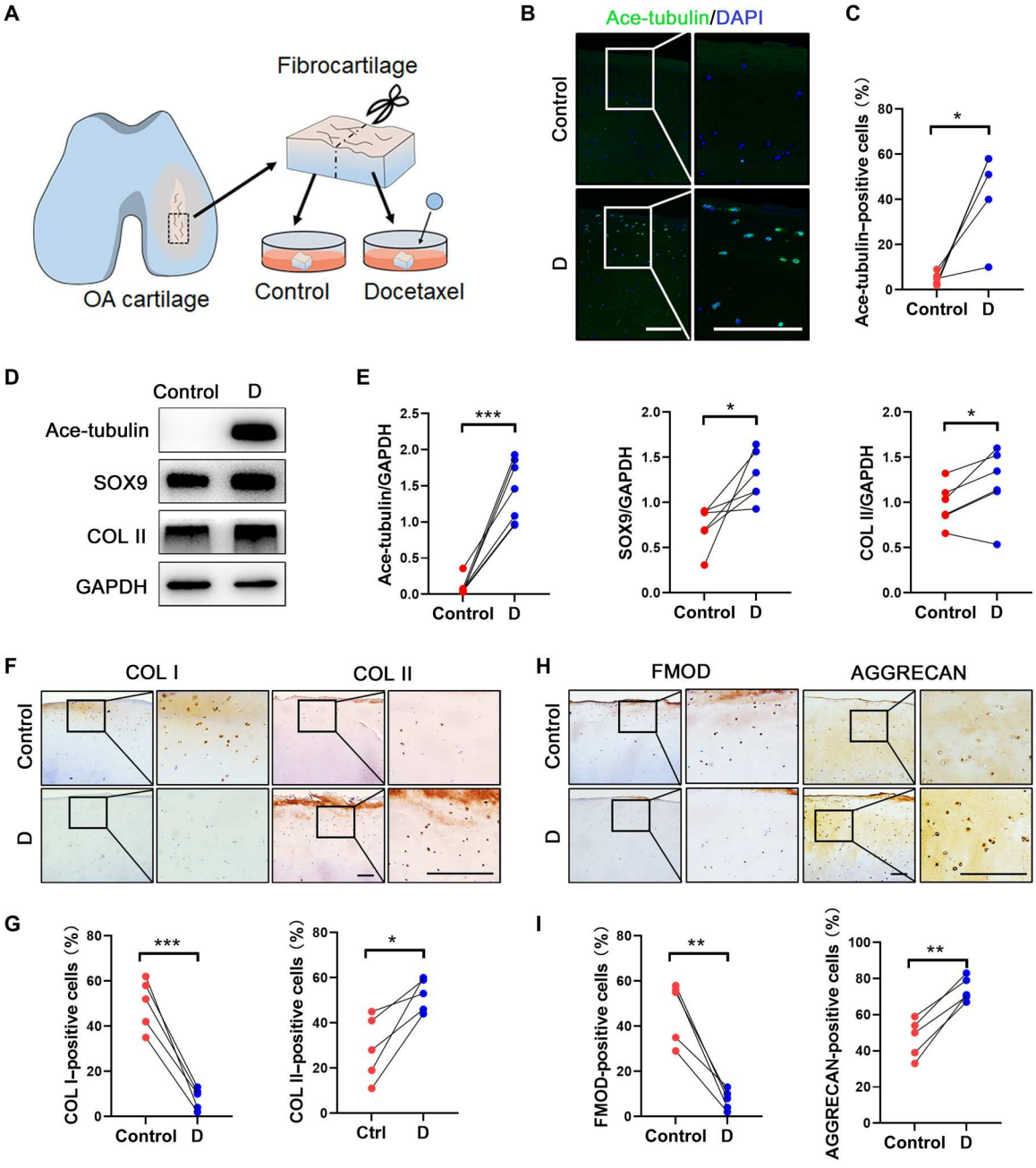

Fig. 6. The effect of microtubule stabilization on the fibrocartilage in human OA. (**A**) Schematic illustration showing the experiment for microtubule stabilization on the human OA fibrocartilage. The fibrocartilage was harvested from the femoral condyle of OA patients and then divided it into two parts and cultured ex vivo for D treatment for 1 weeks and control. (**B**) Immunofluorescent staining for ace-tubulin in the cartilage ex vivo with or without D treatment. Enclosed areas are enlarged in below panels. Scale bars, 200 μm. (**C**) Quantification of ace-tubulin–positive cells of (B) ($n = 4$). (**D**) Western blot analysis for ace-tubulin, SOX9 and COL II of the cartilage ex vivo with or not with D treatment. (**E**) Quantification of data D ($n = 6$). (**F** and **H**) Immunohistochemical staining for COL I, COL II, FMOD, and AGGRECAN in the cartilage ex vivo with or without D treatment. Enclosed areas are enlarged in right panels. Scale bars, 500 μm. (**G** to **I**) Quantification of COL I– and COL II– (G) positive cells of (F) and FMOD- and AGGRECAN-positive (I) cells of (H) ($n = 5$). Data are represented as the means ± SD. *$P < 0.05$, **$P < 0.01$, and ***$P < 0.001$.

needed for promoting the clinical translatability of microtubule stabilization on fibrocartilage hyalinization.

To verify the effect of microtubule stabilization on fibrocartilage hyalinization in vivo, we constructed the rat cartilage injury model to induce fibrocartilage formation and designed a thermosensitive docetaxel-loaded injectable hydrogel (D-PDP@MC-Gel) for targeting fibrocartilage. To effectively modify fibrocartilage in situ, a cartilage engineering strategy for targeting articular fibrocartilage is necessary. In addition, injectable scaffolds can be delivered in a minimally invasive manner via direct injection (*31*). Methylcellulose was used to form a thermo-reversible hydrogel to achieve the sol-gel transition of hydrogel (*32*, *33*). The dosage of docetaxel (75

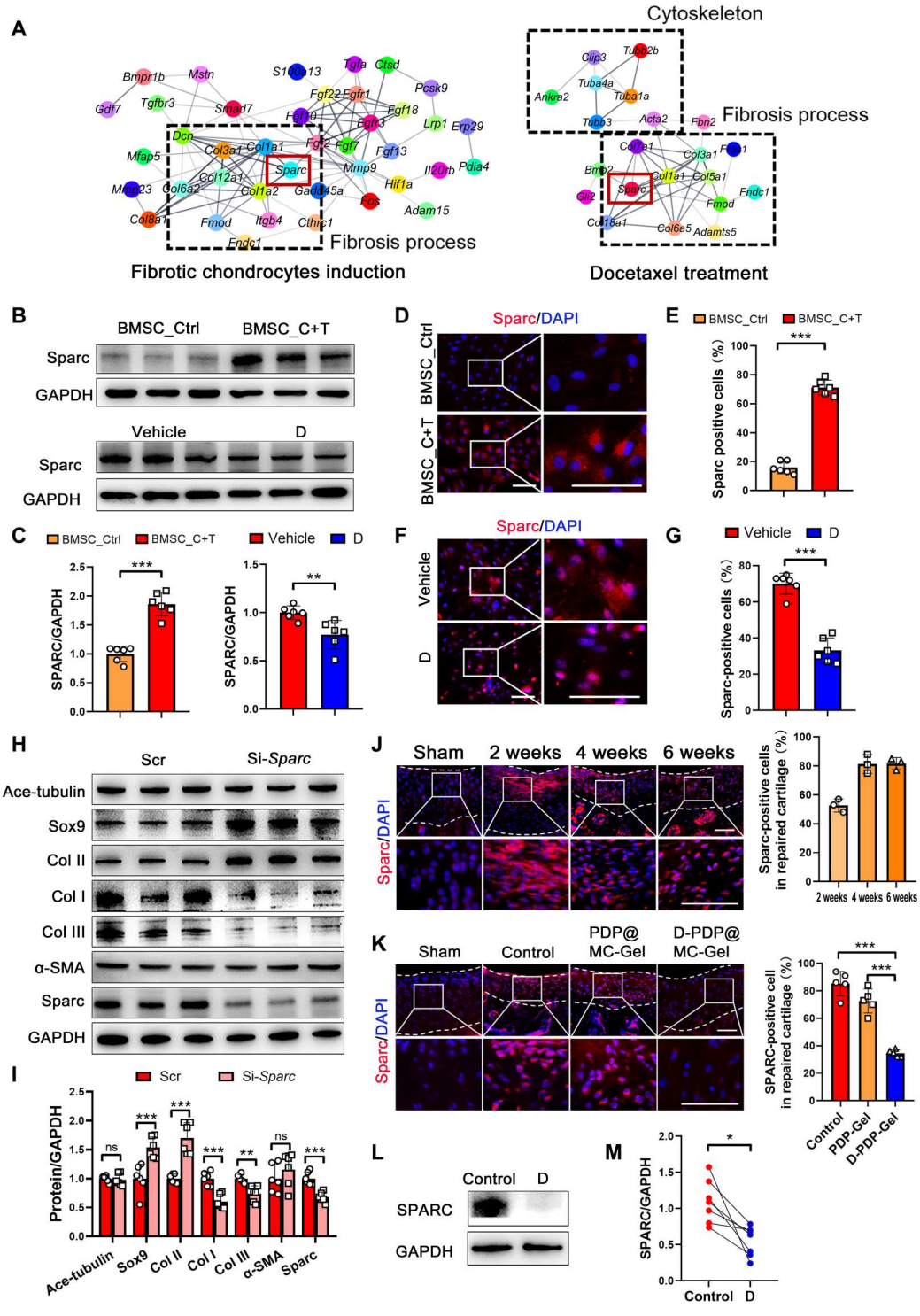

Fig. 7. The mechanism of Sparc in the fibrocartilage hyalinization. (**A**) PPIs of differentially expressed genes. Left: Fibrocartilage chondrocytes introduction. Right: D treatment. (**B**) Western blot analysis for Sparc in the BMSC with or without CTGF and TGF-β1 treatment (B) and in the iFCs with or without D (C). (**C**) Quantification of (B) ($n = 6$). Immunofluorescent staining for Sparc in the BMSC with or without CTGF and TGF-β1 treatment (**D**) and in the iFCs with or without D (**F**). Enclosed areas are enlarged in right panels. Scale bar, 100 μm. Quantification of Sparc-positive cells of (D) (**E**) and (F) (**G**) ($n = 6$). (**H**) Western blot analysis for ace-tubulin, Sox9, Col II, Col I, Col III, α-SMA, and Sparc in the BMSCs under the induction of CTGF and TGF-β1 with or without the transfection of siRNA for Sparc knockdown. (**I**) Quantification of data H ($n = 6$). ns, not significant. (**J**) Immunofluorescent staining for Sparc of the fibrocartilage during the cartilage repair. Enclosed areas are enlarged in below panels. Scale bar, 100 μm. Quantification of Sparc-positive cells in the fibrocartilage in the cartilage defect ($n = 3$). (**K**) Immunofluorescent staining for Sparc of the fibrocartilage in the cartilage defect treated with D-PDP@MC-Gel and PDP@MC-Gel. Enclosed areas are enlarged in below panels. Scale bar, 100 μm. Quantification of Sparc-positive cells in the fibrocartilage in the cartilage defect ($n = 5$). (**L**) Western blot analysis for Sparc of the cartilage ex vivo with or without D treatment. (**M**) Quantification of the Western blot analysis ($n = 6$). Data are represented as the means ± SD. $^*P < 0.05$, $^{**}P < 0.01$, and $^{***}P < 0.001$.

mg/m^2) in the clinic is based on systematic application (*34*). Whereas, the optimal strategy for local delivery of docetaxel was largely unclear. The excessive docetaxel would influence the proliferation of cells and even kill the FCs in fibrocartilage directly, which leads to the failure of cartilage regeneration. In this study, 10 μg of docetaxel was loaded in the 50 μl of MC-Gel (25 μg/kg) for a single intra-articular injection. Our data showed that the MC-Gel could effectively maintain the release of docetaxel and protect docetaxel from degradation by temperature and pH. Furthermore, a low concentration of docetaxel in the joint could be maintained because it could remain in MC-Gel for at least 30 days, which decreased the toxicity of docetaxel. In addition, the sustained release of docetaxel permitted reduced dosing frequency and improved compliance.

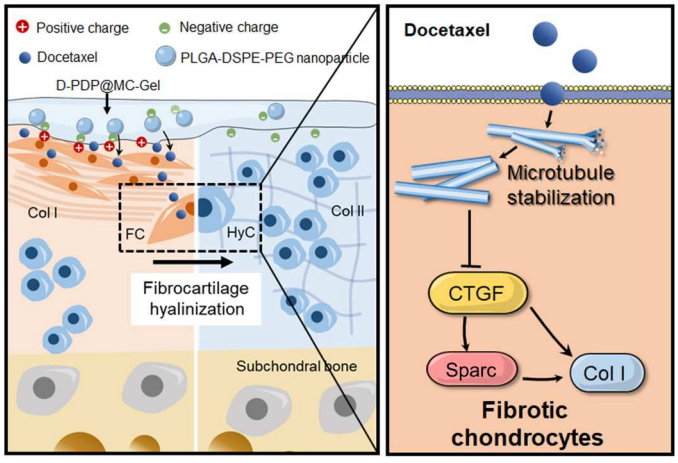

Fig. 8. Schematic of articular fibrocartilage-targeted therapy by microtubule stabilization. Fibrocartilage was modified in situ by microtubule stabilization via docetaxel loaded hydrogel. The transformation of fibrocartilage toward hyaline cartilage by microtubule stabilization was through regulating Sparc. HyC, Hyaline chondrocytes.

The examination of key organs and the weight of rats illustrated the safety of this dosage of docetaxel and MC-Gel.

In the early stage (2 weeks after surgery), a lot of cells were densely distributed in the cartilage defect and produced the initial matrix of repaired tissue (Fig. 1B and fig. S1A). The proliferation and migration of cells into cartilage defect are important to generate the natural source of cells and matrix scaffold for hyaline cartilage production. In addition, we also observed that there were a dense fibril matrix and relatively sparsely distributed cells in the repaired cartilage at 6 weeks after surgery (Fig. 1B and fig. S1A), which provided a barren microenvironment for regeneration. Therefore, the D-PDP@MC-Gel was applied into the knee joint at 4 weeks after cartilage injury surgery. Chondrocytes in the repaired area of fibrocartilage exhibited highly expressed ace-tubulin after the application of D-PDP@MC-Gel, indicating the successful release of docetaxel toward FCs and effective microtubule stabilization. Considering the negatively charged nature of the cartilage ECM, positively charged systems were used to overcome the obstruction of cartilage in previous research, such as avidin and positively charged nanocarrier (*35*, *36*). Our result indicated that a positively charged protein, transferrin, was highly expressed in the fibrocartilage. The positive charge of transferrin damaged the negatively charged environment established by the proteoglycan in healthy cartilage ECM (*27*), which could provide a molecular anchor for drug carriers with the negative surface charge for targeting fibrocartilage (*28*). The DSPE-PEG-COOH carried by docetaxel-loaded PLGA provided negative charge to adhere fibrocartilage to release drug and avoid affecting healthy cartilage and other tissues in the synovial joint. Notably, the fibrocartilage in the repaired area was modified to hyaline cartilage, which was indicated by robustly expressed Col II and aggrecan and substantially decreased expression of Col I and Fmod, two canonical fibrocartilage markers (*37*). These results suggest that the utilization of D-PDP@MC-Gel was effective for docetaxel playing its role in microtubule stabilization in fibrocartilage. Although we achieved the conversion from fibrocartilage to hyaline cartilage and identified the feasibility of fibrocartilage hyalinization, there are issues that should be of concern in future studies: (i) What is the optimal timing of introducing the docetaxel for fibrocartilage hyalinization? (ii) Whether the phenotype of hyaline cartilage could be maintained after docetaxel using up? (iii) What is the difference of the mechanical property pre and post fibrocartilage hyalinization? Furthermore, there are some limitations in the study of rat cartilage injury model. The growth plate still exists under the articular cartilage of rodents, which may lead to increase the intrinsic regenerative ability of cartilage. In addition, the gait and biomechanical environment of rats greatly differ from that of human. Moreover, the size of joint and the thickness of cartilage also hinder the examination of the biomechanical advantage of neocartilage transferred from cartilage. Therefore, to reflect the more specific information of transformation process of fibrocartilage and the characteristics of neocartilage, such as the changes of ECM organization and biomechanical feature, the research of fibrocartilage hyalinization in larger animals is necessary in the future.

The key mechanism of fibrocartilage hyalinization by microtubule stabilization was associated with Sparc. The expression of Sparc is closely aligned with the synthesis of fibrillar collagens, especially Col I (*38*), which was consistent with the PPI analysis of Sparc in our data. It was reported that Sparc was critically required for maturation of FCs and the enthesis development of many connective tissues (*39*, *40*). Our results revealed that the production of CTGF and the process of fibrocartilage formation in vivo both contributed to the increased expression of Sparc, suggesting that Sparc played an important role in fibrocartilage formation. Moreover, RNA sequencing revealed that the Sparc expression showed opposite alteration during the fibrosis induction and microtubule stabilization. These data illustrated that the effect of microtubule stabilization on reverse cartilage fibrosis was based on the mechanism of inhibiting Sparc. Furthermore, we also found that microtubule stabilization reduced the expression of CTGF both in vivo and in vitro. Our present finding suggests that the inhibition of Sparc and CTGF under the condition of microtubule stabilization is the critical mechanism of fibrocartilage hyalinization.

In conclusion, the present study investigated the feasibility of modifying fibrocartilage into hyaline cartilage in situ, suggesting that fibrocartilage hyalinization was a practical and promising strategy for cartilage regeneration. This study represented the preliminary attempt and investigation of fibrocartilage hyalinization, and more possible approaches and specific mechanisms remain to be explored in the future.

MATERIALS AND METHODS

Ethics statement

All surgical operation, drug application, and postoperative care of animal were carried out strictly according to the guidelines of Animal Center of Nanjing Drum Tower Hospital, the affiliated Hospital of Nanjing University (2020AE02013). All experimental procedures in this study involved in human tissue samples followed the guideline of Declaration of Helsinki (*41*). The experiment is involved in the collection, and experiments of cartilage from patients with OA were already approved by the Ethical Committee of the Nanjing Drum Tower Hospital, the affiliated Hospital of Nanjing University (2020-156-01) and strictly complied with the guidelines of the Institutional Animal Care and Use Committee.

Human cartilage sample collection

Seven human cartilage tissues were acquired from patients with clinical OA who received total knee replacement (65 to 74 years old, Kellgren-Lawrence grade IV). One of them was used for histological analysis, and the remaining six were used to perform ex vivo cartilage tissue culture.

Animal study

Adult male Sprague-Dawley rats (240 to 260 g, $n = 32$) were purchased from the Animal Center, Nanjing Medical University (Jiangsu, China). All animals were acclimated for 1 week before all experiments or operations. Full-thickness cartilage defects in the femoral trochlear groove (2.0 mm in diameter, 3.0 mm in depth) were constructed in the right knee of 24 rats via an osteochondral transplantation instrument, and eight rats received a sham operation. Three rats of the sham group and 12 rats of the operated group were used to analyze fibrocartilage formation in the process of cartilage repair. The operated animals were euthanized at 2, 4, and 6 weeks after surgery, respectively ($n = 3$ each). The remaining animals were used to investigate the effect of microtubule stabilization on fibrocartilage hyalinization. The rats were randomly divided into four groups ($n = 5$ each): sham, control (cartilage injury), hydrogel control, and docetaxel-loaded hydrogel groups. The normal saline, PDP@MC-Gel, and D-PDP@MC-Gel were delivered to rats with cartilage injury via intra-articular injection at 4 weeks after operation, and the right knee samples of rats were acquired at 4 weeks after treatment.

Cell culture and fibrotic induction

To establish primary BMSCs culture, the fresh BM samples were collected from the tibia and femur of rats (2 weeks after birth). After filtration and centrifugation, the cells were placed in Dulbecco's modified Eagle's medium (DMEM)–low glucose (LG) (1 g/liter; Gibco, MA, USA). The cells (passage 0) were cultured in the cell incubator with 37°C temperature and 5% CO_2.

When the BMSCs were cultivated to passage 1, the culture medium was replaced by chondrogenic medium, which consisted of L-ascorbic acid-2 phosphate (Aladdin, Shanghai, China), proline (40 μg/ml; Aladdin), 100 mM sodium pyruvate (Aladdin), 10^{-7} M dexamethasone (Sigma-Aldrich, MO, USA), ITS Premix (Sigma-Aldrich), 2% fetal bovine serum (Gibco), and 1% penicillin-streptomycin (Gibco) in DMEM-LG basic medium. Then, the cells were induced by CTGF (100 ng/ml; PeproTech, NJ, USA) for 1 week followed by TGF-β1 (5 ng/ml; PeproTech).

RNA sequencing and analysis

The RNA of cells was first extracted (BMSC_Ctrl versus BMSC_C+T and iFC_vehicle versus iFC_D; $n = 3$ each). After quality control of RNA, the Illumina RNA libraries were constructed with the NEBNext Ultra RNA Library Prep Kit. The RNA library was sequenced by Illumina NovaSeq platform, and then 150–base pair paired-end reads were produced. In-house Perl scripts were used to process all raw data of fastq format, and then the clean data were acquired with strictly quality control. The Hisat2 was chosen as a mapping tool to construct the database of splice junctions following the gene model annotation file.

A differential expression analysis of cells (BMSC_Ctrl versus BMSC_C+T and iFC_vehicle versus iFC_D; $n = 3$ each) was performed using the DESeq2 R package (1.16.1). For controlling the false discovery rate, the Benjamini and Hochberg's approach was performed to adjust the resulting P values. The genes with an adjusted P value less than 0.05 tested by DESeq2 were considered differentially expressed. GO enrichment analysis based on the differentially expressed genes was performed by the clusterProfiler R package. GO terms with adjusted P value < 0.05 were assigned as significantly enriched by differential expressed genes. GSEA was implemented by clusterProfiler R package. PPI analysis based on the differentially expressed genes was performed according to the STRING database.

Western blot analysis

The proteins of cells and tissues were extracted by radioimmunoprecipitation assay lysis buffer. The total protein of cells was separated in SDS–polyacrylamide gels and then transferred toward a polyvinylidene fluoride (PVDF) membrane (Bio-Rad, Hercules, CA, USA). After that, the PVDF membranes were incubated in the 5% (w/v) milk (Bio-Rad) that was used for blocking for 1 hour at room temperature and transferred to the primary antibodies overnight at 4°C. The information of primary antibody was listed at table S1. The membranes were further incubated with horseradish peroxidase (HRP)–conjugated secondary antibodies for 1 hour. All protein signals on membranes were detected using a ChemiDoc XRS+ Imaging System (Tanon, Shanghai, China). All experiments were repeated three times.

Preparation of D-PDP NPs and D-PDP@MC-Gel

The D-PDP NPs were prepared by modified one-pot nanoprecipitation methods. Briefly, 50 mg of PLGA and 5 mg of docetaxel were dissolved in 1 ml of dichloromethane and then added dropwise into 4 ml of deionized (DI) water containing 4 mg of lecithin and 8 mg of DSPE-PEG-COOH under stirring. After 12 hours, the residual acetonitrile was removed by continuous stirring. The reaction solution further removed uncoated docetaxel by centrifugation under 10,000 rpm for 5 min. After that, the D-PDP NPs were collected and lyophilized.

Twelve weight % (wt %) MC solutions were used to prepare the hydrogel. In addition, 4 wt % $Na_2HPO_4{\cdot}12H_2O$ and 8 wt % xylitol were used. All the powder was added in 60°C DI water and stirred for 30 min. Then, the solution was put in 4°C for 12 hours. After cooling, the NPs were added into MC-Gel.

Characterization of NPs and hydrogel

Dynamic light scattering and zeta potential measurements were implemented via a Malvern Zetasizer Nano ZS Instrument. SEM imaging was constructed by a Quanta 200 SEM (Quanta 200). G' and G'' were measured by Modular Advanced Rheometer System (Thermo Fisher Scientific HAAKE MARS, MA, USA).

The sustaining release solutions were collected in different time points under 6 ml of saline. Furthermore, the docetaxel amount in NPs and release solution was quantified by HPLC (Agilent Technologies 1260 Infinity), which is equipped with reverse-phase HPLC column (Sepax GP-C18). The acetonitrile/water (42:58, v/v) mixture was used as a mobile phase, and the flow rate was 1 ml/min and then detected with an ultraviolet at 270 nm.

Histological and microscopic analyses

Cartilage samples from rat femur and patients with OA were incubated in 4% (v/v) paraformaldehyde for 24 hours. After

decalcification, the samples were further embedded in the paraffin and cut into 3-μm sections. The sections were then performed with SO–Fast Green staining and hematoxylin and eosin staining. The histological results of each group were accessed according to the International Cartilage Repair Society visual histological evaluation scoring system (*42*).

Immunofluorescent and immunohistochemical staining analysis

The sections of animals and human OA cartilage were incubated in the primary antibodies overnight under 4°C. The information of primary antibody was listed at table S1. FITC- or tetramethyl rhodamine isothiocyanate (TRITC)–conjugated secondary antibodies were used for sections for 1 hour under a dark condition for immunofluorescent staining. While for immunohistochemical staining, the sections were incubated with HRP-conjugated secondary antibodies. Images of stained sections were captured by a fluorescence microscope (Zeiss, Heidelberg, Germany). All experiments were repeated three times.

Cell immunofluorescent staining

After being fixed in 4% paraformaldehyde, the cells were incubated in 0.1% Triton X-100. Cells were blocked with 5% bovine serum album (BSA) for 1 hour at 37°C and then incubated with primary antibodies overnight at 4°C. The information of primary antibody was listed at table S1. The cells were then incubated with FITC- or TRITC-conjugated second antibodies and further labeled with 4′,6-diamidino-2-phenylindole. Each slide was observed by fluorescence microscope (Zeiss). All experiments were repeated three times.

Pellet and micro-mass cultures

The pellets containing 5×10^5 cells were cultured in a centrifuge tube for 3 weeks with chondrogenic medium supplemented with TGF-β1 (10 ng/ml; PeproTech) and bone morphogenetic protein 2 (500 ng/ml; PeproTech). As for the micro-mass culture, the cell mass containing 5×10^5 cells were planted at the center of the 12-well plate and cultured with chondrogenic medium supplemented with TGF-β1 (10 ng/ml) for 2 weeks.

Micro–computed tomography

The microstructure of femurs of rat was examined by using the micro-CT scanner (mCT80, Scanco Medical AG). The scanner was set at a 114-μA current, a 70-kV voltage, and a resolution of 15.6 μm per pixel. The images of 3D reconstruction were performed and captured with Scanco Medical software.

siRNA transfection

siRNA against the rat *Sparc* was synthesized according to the following sequence: sense: 5-CUGGAUCAGCACCCGAUUGAUdTdT-3; antisense: 5-AUCAAUCGGGUGCU GAUCCAGdTdT-3 (Hippobio, Zhejiang, China). When BMSCs were grown to approximately 70% confluence, the cells were transfected with either negative control siRNA or 50 nM siRNA-*Sparc* supplemented with Lipofectamine 3000 for 12 hours (Thermo Fisher Scientific).

Statistical analysis

Statistical analysis was conducted using the GraphPad Prism software (version 8.0). All data were expressed as means ± SD. For the comparison of mean values between two groups, paired or unpaired two-tailed Student's *t* test was used. One-way analysis of variance (ANOVA) followed by Tukey's post hoc tests were used to assess the statistical significance of the mean values of more than two groups. Multivariate ANOVA (MANOVA) tests were used to assess the statistical significance of the mean values when there is more than one variable. Differences were considered statistically significant when $P < 0.05$.

Supplementary Materials

This PDF file includes:

Figs. S1 to S4
Table S1

View/request a protocol for this paper from *Bio-protocol*.

REFERENCE AND NOTES

1. C. B. Carballo, Y. Nakagawa, I. Sekiya, S. A. Rodeo, Basic science of articular cartilage. *Clin. Sports Med.* **36**, 413–425 (2017).
2. D. J. Huey, J. C. Hu, K. A. Athanasiou, Unlike bone, cartilage regeneration remains elusive. *Science* **338**, 917–921 (2012).
3. J. Malda, J. Groll, P. R. van Weeren, Rethinking articular cartilage regeneration based on a 250-year-old statement. *Nat. Rev. Rheumatol.* **15**, 571–572 (2019).
4. Y. Krishnan, A. J. Grodzinsky, Cartilage diseases. *Matrix Biol.* **71-72**, 51–69 (2018).
5. A. R. Armiento, M. Alini, M. J. Stoddart, Articular fibrocartilage - Why does hyaline cartilage fail to repair? *Adv. Drug Deliv. Rev.* **146**, 289–305 (2019).
6. M. Benjamin, J. R. Ralphs, Biology of fibrocartilage cells. *Int. Rev. Cytol.* **233**, 1–45 (2004).
7. D. F. Remst, E. N. Blaney Davidson, P. M. van der Kraan, Unravelling osteoarthritis-related synovial fibrosis: A step closer to solving joint stiffness. *Rheumatology (Oxford)* **54**, 1954–1963 (2015).
8. R. Karuppal, Current concepts in the articular cartilage repair and regeneration. *J. Orthop.* **14**, A1–A3 (2017).
9. M. Maldonado, J. Nam, The role of changes in extracellular matrix of cartilage in the presence of inflammation on the pathology of osteoarthritis. *Biomed. Res. Int.* **2013**, 284873 (2013).
10. A. C. Hall, The role of chondrocyte morphology and volume in controlling phenotype-implications for osteoarthritis, cartilage repair, and cartilage engineering. *Curr. Rheumatol. Rep.* **21**, 38 (2019).
11. A. I. Vasara, M. T. Nieminen, J. S. Jurvelin, L. Peterson, A. Lindahl, I. Kiviranta, Indentation stiffness of repair tissue after autologous chondrocyte transplantation. *Clin. Orthop. Relat. Res.* **433**, 233–242 (2005).
12. P. S. Mathieu, E. G. Loboa, Cytoskeletal and focal adhesion influences on mesenchymal stem cell shape, mechanical properties, and differentiation down osteogenic, adipogenic, and chondrogenic pathways. *Tissue Eng. Part B Rev.* **18**, 436–444 (2012).
13. Y. Ilan, Microtubules: From understanding their dynamics to using them as potential therapeutic targets. *J. Cell. Physiol.* **234**, 7923–7937 (2018).
14. H. V. Goodson, E. M. Jonasson, Microtubules and microtubule-associated proteins. *Cold Spring Harb. Perspect. Biol.* **10**, a022608 (2018).
15. G. Borisy, R. Heald, J. Howard, C. Janke, A. Musacchio, E. Nogales, Microtubules: 50 years on from the discovery of tubulin. *Nat. Rev. Mol. Cell Biol.* **17**, 322–328 (2016).
16. J. Ruschel, F. Hellal, K. C. Flynn, S. Dupraz, D. A. Elliott, A. Tedeschi, M. Bates, C. Sliwinski, G. Brook, K. Dobrindt, M. Peitz, O. Brüstle, M. D. Norenberg, A. Blesch, N. Weidner, M. B. Bunge, J. L. Bixby, F. Bradke, Axonal regeneration. Systemic administration of epothilone B promotes axon regeneration after spinal cord injury. *Science* **348**, 347–352 (2015).
17. G. Cappelletti, A. M. Calogero, C. Rolando, Microtubule acetylation: A reading key to neural physiology and degeneration. *Neurosci. Lett.* **755**, 135900 (2021).
18. A. J. Matamoros, P. W. Baas, Microtubules in health and degenerative disease of the nervous system. *Brain Res. Bull.* **126**, 217–225 (2016).
19. K. W. Prins, L. Tian, D. Wu, T. Thenappan, J. M. Metzger, S. L. Archer, Colchicine depolymerizes microtubules, increases junctophilin-2, and improves right ventricular function in experimental pulmonary arterial hypertension. *J. Am. Heart Assoc.* **6**, e006195 (2017).
20. M. A. Callender, E. S. Antonarakis, Rheumatoid arthritis masked by docetaxel chemotherapy in a patient with ovarian carcinoma. *J. Clin. Rheumatol.* **14**, 121 (2008).

21. J. Li, Z. Sun, Z. Lv, H. Jiang, A. Liu, M. Wang, G. Tan, H. Guo, H. Sun, R. Wu, X. Xu, W. Yan, Q. Jiang, S. Ikegawa, D. Shi, Microtubule stabilization enhances the chondrogenesis of synovial mesenchymal stem cells. *Front. Cell Dev. Biol.* **9**, 748804 (2021).
22. C. H. Lee, S. A. Rodeo, L. A. Fortier, C. Lu, C. Erisken, J. J. Mao, Protein-releasing polymeric scaffolds induce fibrochondrocytic differentiation of endogenous cells for knee meniscus regeneration in sheep. *Sci. Transl. Med.* **6**, 266ra171 (2014).
23. C. H. Lee, B. Shah, E. K. Moioli, J. J. Mao, CTGF directs fibroblast differentiation from human mesenchymal stem/stromal cells and defines connective tissue healing in a rodent injury model. *J. Clin. Invest.* **125**, 3992 (2015).
24. S. Thysen, F. P. Luyten, R. J. Lories, Loss of Frzb and Sfrp1 differentially affects joint homeostasis in instability-induced osteoarthritis. *Osteoarthr. Cartil.* **23**, 275–279 (2015).
25. Y. Xie, A. Zinkle, L. Chen, M. Mohammadi, Fibroblast growth factor signalling in osteoarthritis and cartilage repair. *Nat. Rev. Rheumatol.* **16**, 547–564 (2020).
26. X. Wang, P. A. Manner, A. Horner, L. Shum, R. S. Tuan, G. H. Nuckolls, Regulation of MMP-13 expression by RUNX2 and FGF2 in osteoarthritic cartilage. *Osteoarthr. Cartil.* **12**, 963–973 (2004).
27. C. H. Evans, Drug delivery to chondrocytes. *Osteoarthr. Cartil.* **24**, 1–3 (2016).
28. B. Tirosh, N. Khatib, Y. Barenholz, A. Nissan, A. Rubinstein, Transferrin as a luminal target for negatively charged liposomes in the inflamed colonic mucosa. *Mol. Pharm.* **6**, 1083–1091 (2009).
29. Y. N. Cao, L. L. Zheng, D. Wang, X. X. Liang, F. Gao, X. L. Zhou, Recent advances in microtubule-stabilizing agents. *Eur. J. Med. Chem.* **143**, 806–828 (2018).
30. A. D. Tangutur, D. Kumar, K. V. Krishna, S. Kantevari, Microtubule targeting agents as cancer chemotherapeutics: An overview of molecular hybrids as stabilizing and destabilizing agents. *Curr. Top. Med. Chem.* **17**, 2523–2537 (2017).
31. J. Li, G. Chen, X. Xu, P. Abdou, Q. Jiang, D. Shi, Z. Gu, Advances of injectable hydrogel-based scaffolds for cartilage regeneration. *Regen. Biomater.* **6**, 129–140 (2019).
32. Z. Liu, P. Yao, Injectable thermo-responsive hydrogel composed of xanthan gum and methylcellulose double networks with shear-thinning property. *Carbohydr. Polym.* **132**, 490–498 (2015).
33. M. H. Kim, B. S. Kim, H. Park, J. Lee, W. H. Park, Injectable methylcellulose hydrogel containing calcium phosphate nanoparticles for bone regeneration. *Int. J. Biol. Macromol.* **109**, 57–64 (2018).
34. O. Arrieta, F. Barron, L. A. Ramirez-Tirado, Z. L. Zatarain-Barron, A. F. Cardona, D. Diaz-Garcia, M. Yamamoto Ramos, B. Mota-Vega, A. Carmona, M. P. Peralta Alvarez, Y. Bautista, F. Aldaco, R. Gerson, C. Rolfo, R. Rosell, Efficacy and safety of pembrolizumab plus docetaxel vs docetaxel alone in patients with previously treated advanced non-small cell lung cancer: The PROLUNG phase 2 randomized clinical trial. *JAMA Oncol.* **6**, 856–864 (2020).
35. A. G. Bajpayee, C. R. Wong, M. G. Bawendi, E. H. Frank, A. J. Grodzinsky, Avidin as a model for charge driven transport into cartilage and drug delivery for treating early stage post-traumatic osteoarthritis. *Biomaterials* **35**, 538–549 (2014).
36. K. A. Elsaid, L. Ferreira, T. Truong, A. Liang, J. Machan, G. G. D'Souza, Pharmaceutical nanocarrier association with chondrocytes and cartilage explants: Influence of surface modification and extracellular matrix depletion. *Osteoarthr. Cartil.* **21**, 377–384 (2013).
37. Y. A. Rim, J. H. Ju, The role of fibrosis in osteoarthritis progression. *Life (Basel)* **11**, 3 (2020).
38. E. M. Rosset, A. D. Bradshaw, SPARC/osteonectin in mineralized tissue. *Matrix Biol.* **52-54**, 78–87 (2016).
39. T. Wang, A. Wagner, R. Gehwolf, W. Yan, F. S. Passini, C. Thien, N. Weissenbacher, Z. Lin, C. Lehner, H. Teng, C. Wittner, Q. Zheng, J. Dai, M. Ni, A. Wang, J. Papadimitriou, T. Leys, R. S. Tuan, S. Senck, J. G. Snedeker, H. Tempfer, Q. Jiang, M. H. Zheng, A. Traweger, Load-induced regulation of tendon homeostasis by SPARC, a genetic predisposition factor for tendon and ligament injuries. *Sci. Transl. Med.* **13**, eabe5738 (2021).
40. J. E. Murphy-Ullrich, E. H. Sage, Revisiting the matricellular concept. *Matrix Biol.* **37**, 1–14 (2014).
41. General Assembly of the World Medical, World Medical Association declaration of Helsinki: Ethical principles for medical research involving human subjects. *J. Am. Coll. Dent.* **81**, 14–18 (2014).
42. M. P. van den Borne, N. J. Raijmakers, J. Vanlauwe, J. Victor, S. N. de Jong, J. Bellemans, D. B. Saris; International Cartilage Repair Society, International Cartilage Repair Society (ICRS) and Oswestry macroscopic cartilage evaluation scores validated for use in Autologous Chondrocyte Implantation (ACI) and microfracture. *Osteoarthr. Cartil.* **15**, 1397–1402 (2007).

Acknowledgments

Funding: This work was supported by the National Key R&D Program of China (2018YFC1105904), the National Key Program of NSFC (81730067), the National Science Foundation of China (81772335, 81941009, and 81802196), the Natural Science Foundation of Jiangsu Province, China (BK20180127), the Jiangsu Provincial Key Medical Talent Foundation, and the Six Talent Peaks Project of Jiangsu Province (WSW-079). **Author contributions:** J.L. conducted the most assays and acquired and analyzed data. C.C. participated the design and production of biomaterial for cartilage injury. All authors participated in experiments. D.S. conceived the project and designed the study. J.L. arranged the results and wrote the original manuscript. D.S., J.L., Z. Lv, and Z.S. participated in the review and editing of the study. **Competing interests:** The authors declare that they have no competing interests. **Data and materials availability:** All data needed to evaluate the conclusions in the paper are present in the paper and/or the Supplementary Materials. All RNA sequencing and metadata are available at GEO (https://www.ncbi.nlm.nih.gov/geo/, GSE207148).

Submitted 23 December 2021
Accepted 21 October 2022
Published 18 November 2022
10.1126/sciadv.abn8420